Ionics (2023) 29:4285–4293
https://doi.org/10.1007/s11581-023-05133-5

RESEARCH

Nickel–cobalt layered double hydroxide nanoflakes combined carbonized melamine sponge for high-performance supercapacitors and pressure sensors

Hexiang Hu[1] · Jialun Li[1] · Yi Jiang[2] · Liying Wang[1] · Xijia Yang[1] · Xuesong Li[1] · Wei Lü[1,3]

Received: 11 May 2023 / Revised: 6 July 2023 / Accepted: 17 July 2023 / Published online: 25 July 2023

Abstract

Nickel–cobalt layered double hydroxide (Ni–Co LDH) is a pseudocapacitance electrode material, which has attracted wide attention due to its excellent electrochemical performance, high theoretical capacitance, and a large amount of natural resources. However, the current problem is its poor electrical conductivity and the collapse and stacking of the lamellar structure during the charging and discharging process. In this paper, carbonized melamine sponge (CMS) was prepared by high-temperature calcination, and then, it is compounded with the Ni–Co LDH by further hydrothermal reaction. The resulted Ni–Co LDH nanoflake structure induced the improved electrolyte flow and ion transfer. The Ni–Co LDH@CMS electrode achieved a specific capacitance of 2039.8 mF cm^{-2} and 80.3% capacity retention after 5000 cycles. Then, an all-solid-state flexible asymmetric supercapacitor (ASC) was prepared by Ni–Co LDH@CMS as a cathode. When the power density is 0.699 mW cm^{-2}, the energy density of the ASC is 66.79 μWh cm^{-2}. The capacitor retention rate is as high as 85.2% after 5000 cycles. In addition, Ni–Co LDH@CMS composite was applied to a wearable pressure sensor for monitoring human health, which has a fast response time and recovery time of 20 ms, as well as excellent stability after 5000 cycles. This work indicates that Ni–Co LDH@CMS composite has an excellent prospect as a kind of flexible versatile material.

Keywords Supercapacitors · Pressure sensors · Flexible electrode material · Ni–Co LDH nanoflakes · Carbonized melamine sponge

Introduction

With the rapid progress of science and technology, flexible and wearable electronic devices have gradually become important in daily life, leading to an increasing demand for multi-functional electronic gadgets [1–3]. In recent years, energy storage devices, such as lithium-ion batteries, sodium-ion batteries, and supercapacitors, as well as sensing devices, such as pressure sensors and temperature sensors, have gained a lot of attention in the field of electronics [4–8]. Supercapacitors have attracted significant attention due to their good reversibility and circularity during energy storage processes [9–12]. Moreover, pressure sensors possess remarkable features, such as high response speed, excellent stability, and wide applicability, making them highly useful in fields including medical equipment, human body monitoring, and automatic control [13–15]. To enhance the application ability of electrode materials, designing and improving their performance are a critical challenge. It has been discovered that metal oxides or hydroxides can generate ultra-high pseudocapacitance, which provides promise as an electrode material [16–21]. Among these materials, Ni–Co LDH has attracted great attention due to its outstanding performance, strong redox activity, easy preparation, high specific capacitance (*Cs*), and low price [22–26]. However, limited electrical conductivity and lamellar structure agglomeration during long-term cycling remain issues that need to be addressed to further optimize the performance of Ni–Co LDH.

✉ Wei Lü
lw771119@hotmail.com

[1] Key Laboratory of Advanced Structural Materials, Ministry of Education & Advanced Institute of Materials Science, Changchun University of Technology, Changchun 130012, China

[2] School of Science, Changchun Institute of Technology, Changchun 130012, China

[3] State Key Laboratory of Luminescence and Applications, Changchun Institute of Optics, Fine Mechanics and Physics, Chinese Academy of Sciences, Changchun 130033, China

Carbon-based materials, such as graphene, activated carbon (AC), and CMS, exhibit excellent electrical conductivity and structural stability, making them ideal for combining with metal hydroxides to improve the electrochemical performance of these materials [27–31]. Zou et al. grew Ni–Co LDH nanosheets on a graphene matrix and successfully improved the rate performance and cycle stability of electrode materials [32]. Sun et al. synthesized NiCo-DH@OAC composite material by hydrothermal method using oxidized activated carbon and Ni–Co LDH, which successfully improved the *Cs* and structural stability of electrode materials [33]. Shan et al. prepared Sponge-NiMn hydroxide composite by hydrothermal method and then obtained NiMn oxide supported by porous carbon by calcination, which greatly increased the active reaction area and ensured good cycle stability of the materials [34]. These studies demonstrate that combining carbon-based materials with Ni–Co LDH enhances the stability of the latter while increasing the number of electrochemical reaction active sites, thereby improving the performance of supercapacitors. Melamine sponge is a 3D porous material with low cost, high porosity, low density, compressibility, good flexibility, and elasticity, making it an ideal material with significant practical application potential [35–39]. The higher porosity of the melamine sponge enables faster ion diffusion in the electrolyte and a larger surface area, thus improving the *Cs* of the supercapacitor [40–44]. Combining CMS with Ni–Co LDH is expected to yield a flexible electrode material with outstanding performance.

In the present work, we utilized melamine sponge as raw material and prepared CMS through high-temperature calcination. Then, Ni–Co LDH nanoflakes were prepared by hydrothermal method using CMS as a template. The Ni–Co LDH@CMS composite has the *Cs* of 2039.8 mF cm^{-2}, and its open lamellar structure provides more active sites and promotes ion transfer. Moreover, an all-solid-state flexible ASC was prepared by Ni–Co LDH@CMS cathode, which exhibited good energy density and excellent cycling performance. Furthermore, we prepared a pressure sensor utilizing a Ni–Co LDH@CMS composite material, which shows excellent performance in terms of response speed and stability. Therefore, as a multi-functional material with good electrochemical and mechanical properties, Ni–Co LDH@CMS composite has good application potential in the fields of energy storage and pressure sensing.

Experimental

Preparation of Ni–Co LDH@CMS composite

Preparation of CMS

The melamine sponge was subjected to ultrasonic cleaning with deionized water and ethanol to remove grease and impurities from its surface. Then, the melamine sponge was annealed in a nitrogen atmosphere at 800 °C for 150 min to obtain CMS.

Preparation of Ni–Co LDH@CMS composite

A total of 0.58 g of nickel nitrate hexahydrate, 0.58 g of cobalt nitrate hexahydrate, 0.24 g of urea, and 0.33 g of dimethylimidazole were dissolved in 40 ml of methanol by magnetic stirring. Then, the CMS and the mixed solution were placed together in a 50-ml reactor and heated at 120 °C for 10 h to undergo a hydrothermal reaction. After completion of the reaction, the resulting sample surface was cleaned with a large amount of ionized water and dried at 60 °C for 12 h to obtain the Ni–Co LDH@CMS composite.

Assembly of all-solid-state flexible ASCs

AC anode was obtained by grinding and coating AC, PVDF, and conductive carbon black (8:1:1) on carbon cloth. The PVA/KOH gel film was prepared by dissolving 2.5 g PVA in 25 ml DIW and then adding 3 M KOH. The all-solid-state flexible ASC was assembled with PVA/KOH gel electrolyte, AC anode, and Ni–Co LDH@CMS cathode.

Preparation of the pressure sensor

Ni–Co LDH@CMS is placed on the purchased digital interelectrode and packaged in dust-free paper. The pressure sensor is then assembled by connecting two copper wires to the digital interelectrode through a conductive silver paste.

Results and discussion

Figure 1 is the synthesis procedure of Ni–Co LDH@CMS composites. Flexible MS was calcined at high temperatures to prepare CMS. As a 3D network structure material, it has more obvious voids and good electrical conductivity after carbonization. Then, Ni–Co LDH nanoflakes were prepared on CMS by hydrothermal method. Ni–Co LDH nanoflakes were tightly wrapped on the CMS surface, which enhanced the structural stability and ion transport ability of electrode materials (the photographs of the MS, CMS, and Ni–Co LDH@CMS material are presented in Fig. S1).

Figure 2a shows the X-ray diffraction (XRD) pattern of Ni–Co LDH@CMS. The strong diffraction peak at 29.3° assigned to CMS appears, which shows that CMS after high-temperature calcination has better crystallinity [45].

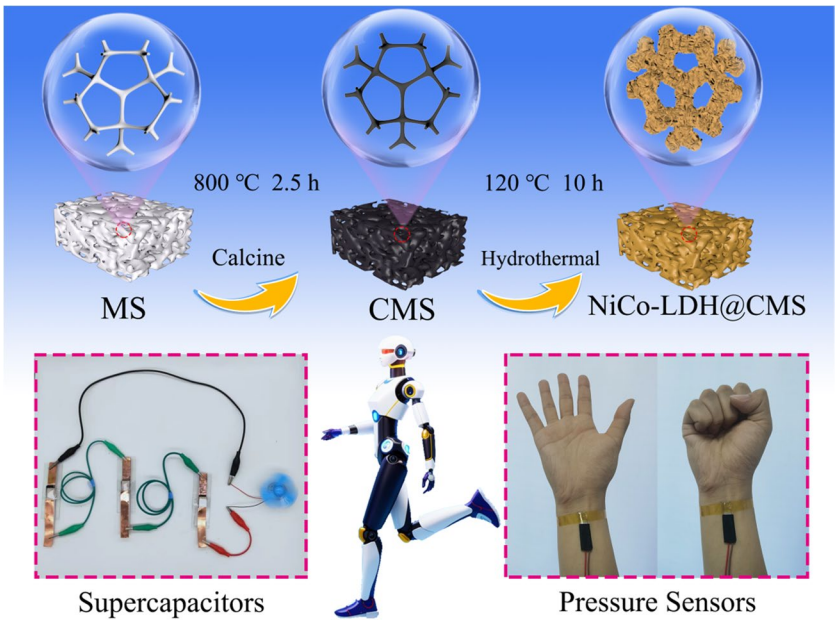

Fig. 1 Schematic illustration of the synthesis process of Ni–Co LDH@CMS composites

The diffraction peaks at 10.85, 22.05, 34.36, 39.06, 43.03, 46.96, and 60.77° can be well attributed to Ni–Co LDH (JCPDS card NO. 40-0216), proving the successful preparation of Ni–Co LDH@CMS composites.

It was further analyzed by X-ray photoelectron spectroscopy (XPS) spectra. Ni 2p, Co 2p, C 1s, and O 1s peaks can be seen in the full XPS spectrum of Fig. 2b. In Fig. 2c, two characteristic peaks of Ni $2p_{1/2}$ and Ni $2p_{3/2}$ of the Ni 2p high-resolution spectrum can be discretized and fitted as two spin-orbit twins. This indicates the presence of Ni^{2+} (872.8 and 855.1 eV) and Ni^{3+} (873.8 and 856.6 eV). Additionally, two peaks at 879.5 and 861.3 eV correspond to the Ni $2p_{1/2}$ and Ni $2p_{3/2}$ states [46]. Figure 2d displays the high-resolution Co 2p spectrum, revealing the presence of Co $2p_{1/2}$ and Co $2p_{3/2}$ that can be discretized into two spin-orbit twins. It can be seen from the spectral results that Co^{2+} (797.2 and 781.1 eV) and Co^{3+} (795.9 and 780.4 eV) coexist. The peaks at 802.4eV and 785.6eV can be attributed to Co $2p_{1/2}$ and Co $2p_{3/2}$ states [47]. For C 1s spectrum in Fig. 2e, it can be fitted by three peaks (C1: 284.3, C2: 285.2, and C3: 287.9 eV),

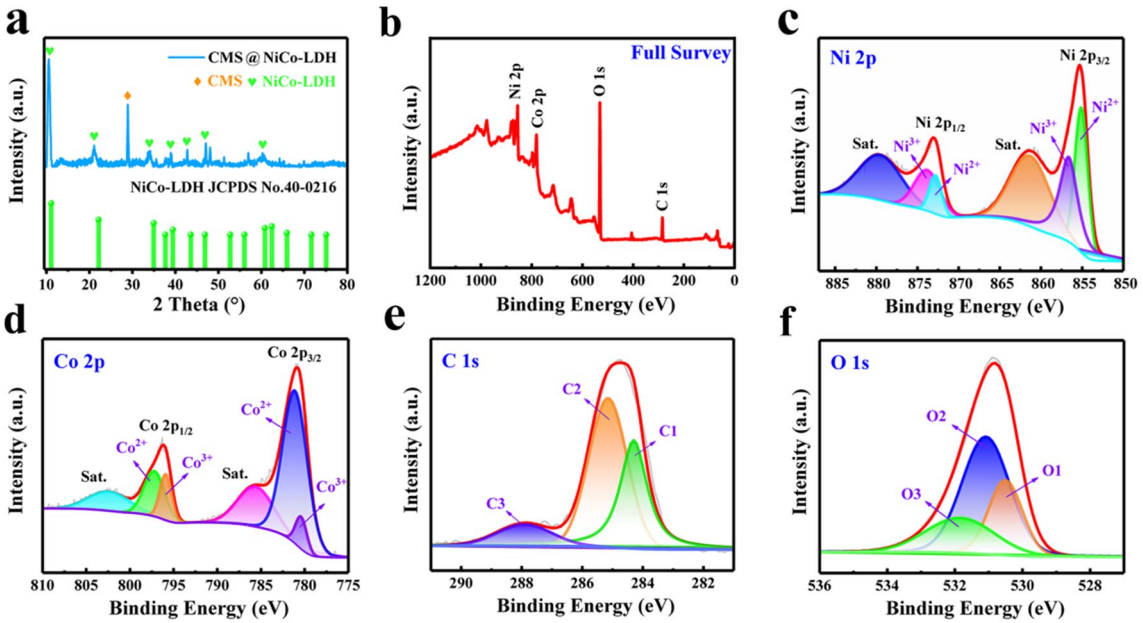

Fig. 2 **a** XRD pattern and **b** XPS survey spectrum of Ni–Co LDH@CMS; high-resolution spectra of **c** Ni 2p, **d** Co 2p, **e** C 1s, and **f** O 1s

corresponding to C=C, C–O, and O=C–O groups, indicating the presence of CMS [48]. Figure 2f presents the high-resolution O 1s spectrum which mainly consists of three peaks (O1: 530.5, O2: 531.1, and O3: 531.8 eV) [49]. The O1, O2, and O3 peaks represent the existence of M–O–H, M–O–M, and H–O–H groups, respectively.

The 3D porous network structure of MS is composed of branched fibers (Fig. 3a–c), and this 3D porous structure is conducive to the transport of ions in the electrolyte solution. Figure 3d–f is the scanning electron microscopy (SEM) images of the Ni–Co LDH@CMS electrode, clearly showing the uniform growth of Ni–Co LDH nanoflakes on the CMS framework. The diameter of the sponge fiber is about 2 μm, while the thickness of the nanoflake can reach the nanoscale. As shown in Fig. 3d, the 3D network structure of CMS still remains unchanged after the hydrothermal reaction. From the SEM images with higher magnification (Fig. 3e, f), it can be seen that the thin nanoflake layers of the sample are staggered between each other, leaving enough space for the electrolyte to fully wet the Ni–Co LDH surface. This structure effectively increases the active area, thereby improving the *Cs* of supercapacitors. In Fig. 3g–k, the Ni, Co, C, and O elements of Ni–Co LDH@CMS are uniformly distributed in the entire structure. Additionally, Fig. S2a displays the nitrogen adsorption and desorption isotherm of Ni–Co LDH@CMS, and the BET theoretical model results indicate that the material possesses a specific surface area of 18.5 m^2 g^{-1}. Fig. S2b illustrates the pore size distribution of Ni–Co LDH@CMS, revealing a rich mesoporous structure with a majority pore size of 30 nm.

To investigate the electrochemical performances of Ni–Co LDH@CMS composites, the cyclic voltammetry (CV), galvanostatic charge and discharge (GCD), and electrochemical impedance spectroscopy (EIS) methods were used for testing and analysis in a three-electrode system with 3 M KOH electrolyte. Figure 4a shows CV curves of Ni–Co LDH@CMS electrode material at different scanning rates. It can be observed that the shape of the CV curve remains good with the increase in scanning rate, which indicates that the Faraday redox reaction occurring on the surface of CMS@NiCo-LDH electrode material has good reversibility. Fig. S3 shows CV curves (5 mV s^{-1}) and GCD curves (1 mA cm^{-2}) of CMS and Ni–Co LDH@CMS. It can be seen that the *Cs* of CMS is negligible compared to the active materials. As shown in Fig. 4b, all GCD curves exhibit a clear voltage plateau during charge and discharge, which can correspond to the redox peak of the CV curve. It has a longer discharge time at 1 mA cm^{-2}, which means a higher *Cs*. In Fig. S4, the *Cs* of Ni–Co LDH@CMS composites is 2039.8, 1767, 1655, 672, 580, and 200 mF cm^{-2} at 1, 2, 4, 6, 8, and 10 mA cm^{-2}, respectively. In addition, the Ni–Co LDH@CMS composites demonstrated competitiveness when compared with other active materials (see Table S1). In order to further explore the electrochemical performance of the Ni–Co LDH@CMS composites, the EIS curve of Ni–Co LDH@CMS is shown Fig. 4c (Fig. S5 shows the equivalent circuit diagram). The

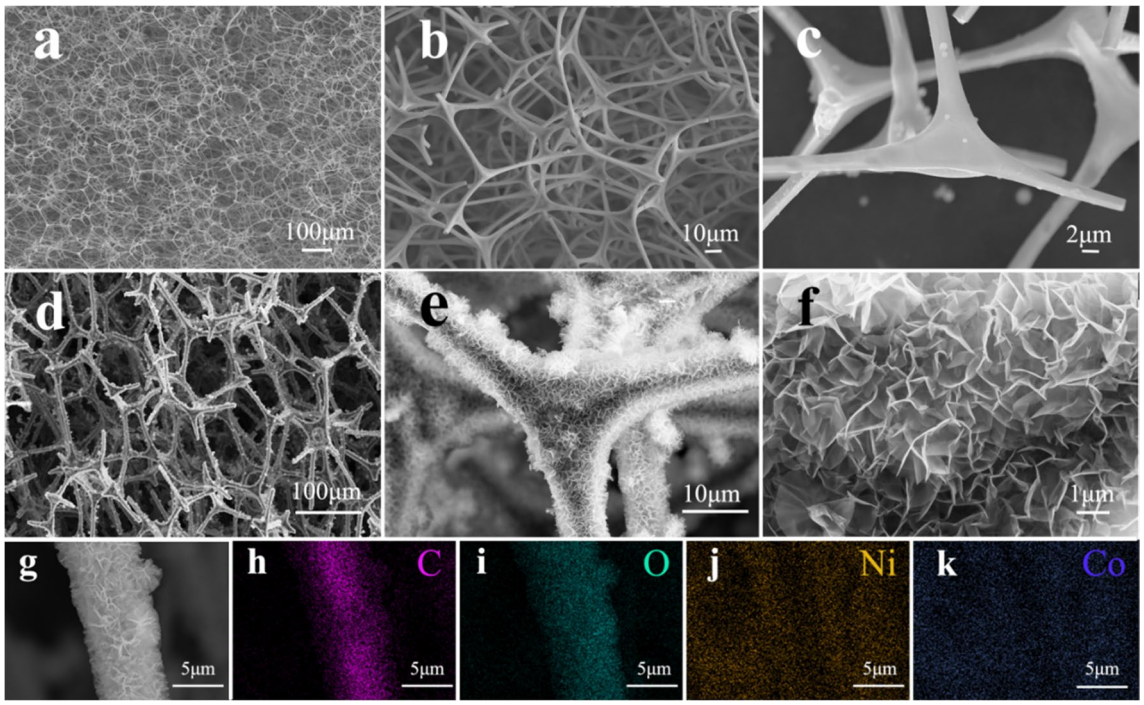

Fig. 3 SEM images of **a–c** CMS and **d–f** Ni–Co LDH@CMS. **g–k** SEM images of element mapping of C, Ni, Co, and O

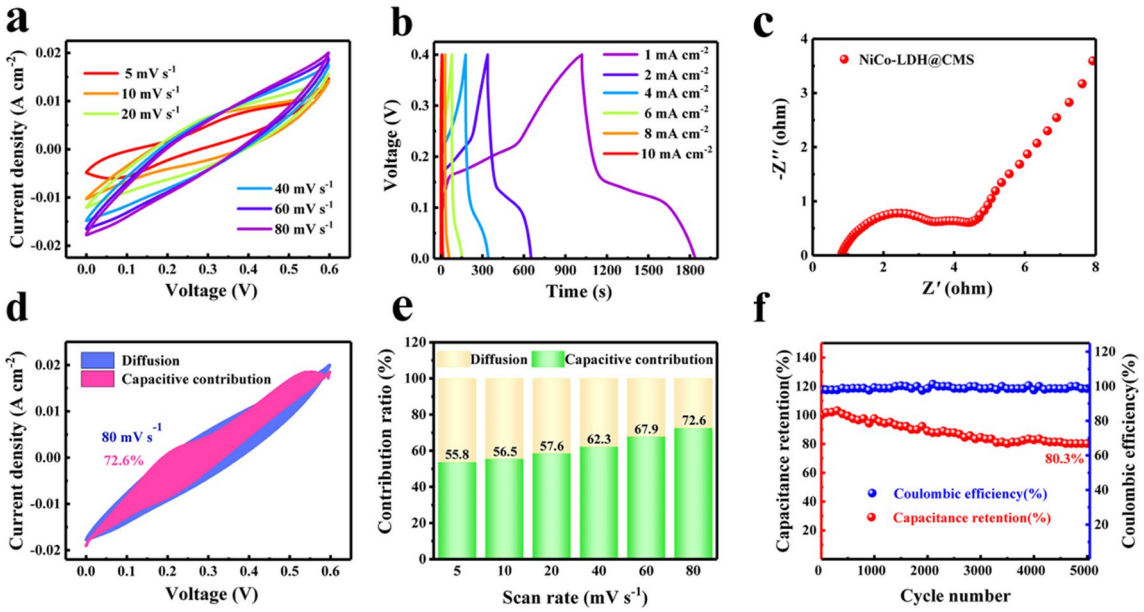

Fig. 4 **a** CV curves of Ni–Co LDH@CMS at different scan rates; **b** GCD curves of Ni–Co LDH@CMS at different current densities; **c** EIS curve of Ni–Co LDH@CMS; **d** capacitive contribution of Ni–Co LDH@CMS at 80 mV s^{-1}; **e** ratio of capacitive controlled and diffusion-controlled contribution at different scan rates; **f** cycling test of Ni–Co LDH@CMS at 20 mA cm^{-2} for 5000 cycles

charge transfer resistance (Rct) is 1.536 Ω, and the equivalent series resistance (Rs) is 0.834 Ω. Its lower resistance shows good ion transfer kinetics of the Ni–Co LDH@CMS composite. In addition, the ratio between capacitance control and diffusion control can be calculated using the formula:

$$I = K_1V + K_2V^{1/2} \quad (1)$$

Here, I represents the total current, K_1V represents the contribution of capacitance control, and $K_2V^{1/2}$ represents the contribution of diffusion control. As depicted in Fig. 4d, the capacitance control contribution of the Ni–Co LDH@CMS electrode is 72.6% at 80 mV^{-1} (the proportion of capacitance control contribution under other scanning rates is shown in Fig. S6). Figure 4e illustrates the capacitance control contribution of the Ni–Co LDH@CMS electrode under different scanning rates. It is evident that the capacitance control process significantly influences the overall capacity, indicating the rapid transfer kinetics of Ni–Co LDH@CMS. In addition, 5000 cycle stability tests were performed at 20 mA cm^{-2}. The coulombic efficiency of Ni–Co LDH@CMS was basically maintained at 100% in Fig. 4f, which indicates that the faradaic redox reaction occurring on the composite surface is highly reversible. A total of 80.3% of the original capacity is still maintained after 5000 cycle tests, indicating its good long-term cycle stability. Fig. S7 (a, b) shows the SEM images of Ni–Co LDH@CMS after 5000 cycles at different magnifications. The layered structure of Ni–Co LDH is well maintained, and there is no collapse or stacking of the layered structure. Therefore, Ni–Co LDH@CMS has good cycle stability.

To investigate the application potential of Ni–Co LDH@CMS, with Ni–Co LDH@CMS as a cathode, AC@CC (carbon cloth) as an anode, and PVA/KOH gel as an electrolyte, an all-solid-state flexible ASC was prepared. In Fig. 5a, the voltage window of AC is −1 to 0 V and that of Ni–Co LDH@CMS is 0–0.6 V (the electrochemical characteristics of the AC anode are shown in Fig. S8). Thus, the voltage range of the combined ASC is up to 1.6 V. A safety voltage of 1.4 V has been chosen to ensure the safety of flexible ASC. Figure 5b shows CV curves of the ASC at different voltage ranges under the condition of 20 mV s^{-1}. The shape of the CV curve is maintained nicely, showing the feasibility of manufacturing 1.4 V ASC. Figure 5c illustrates the GCD curves of the ASCs under different voltage ranges at 5 mA cm^{-2}. And the GCD curves maintain a good shape, indicating its good electrochemical reversibility.

Figure 5d illustrates the device CV curves at different scanning speeds. The CV curve maintains a good shape, indicating its good rate capability. Figure 5e illustrates the GCD curves of the ASCs at various current densities of 1, 2, 4, 6, 8, and 10 mA cm^{-2}. And corresponding calculated Cs of the device is 245.4, 234.6, 204.8, 188.5, 172, and 157.2 mF cm^{-2}, respectively. Fig. S9 shows the Cs of the ASC at different current densities. The performance of Cs in the present work is compared with other reports in Table S1. Even with a 10-fold increase in current density, it can still

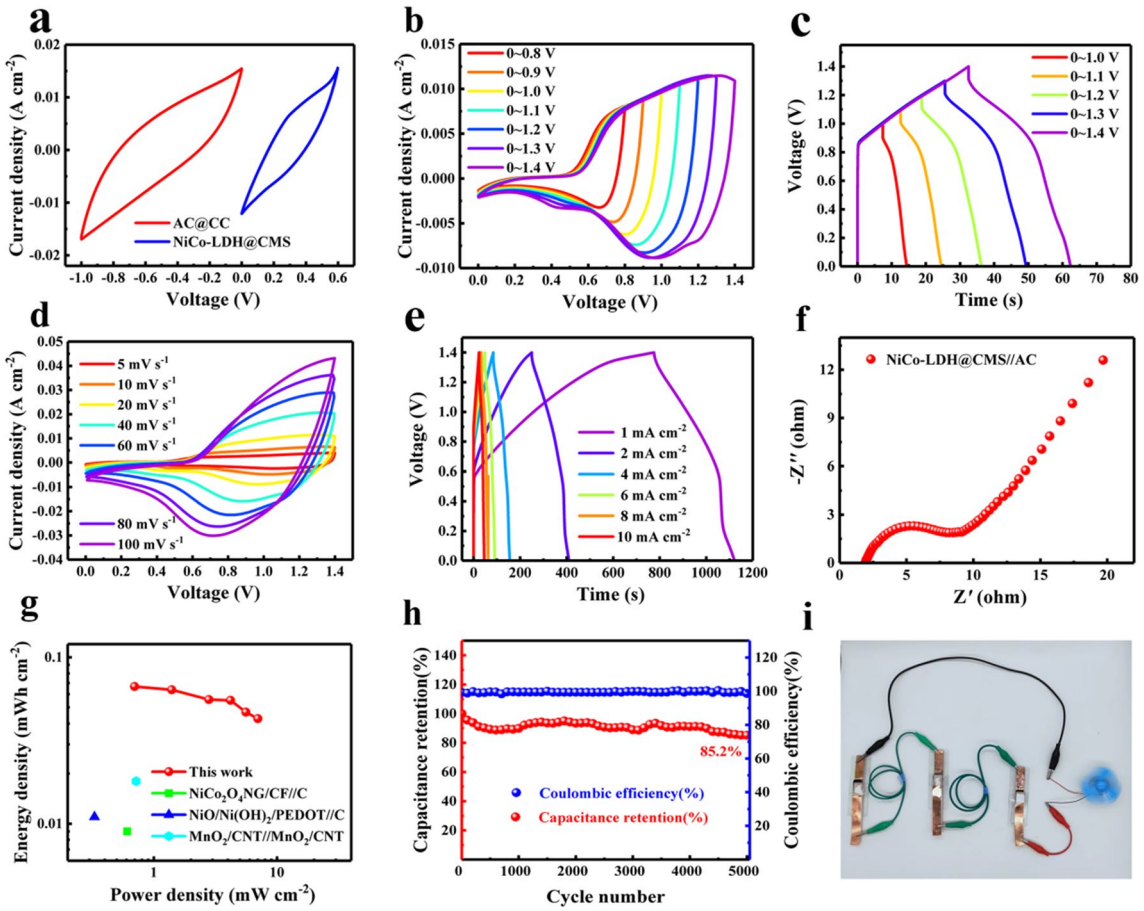

Fig. 5 **a** CV curves of Ni–Co LDH@CMS and AC@CC at 50 mV s^{-1}; **b** CV curves and **c** GCD curves of Ni–Co LDH@CMS//AC all-solid-state flexible ASC in different voltage ranges; **d** CV curves of the ASC at different scanning rates; **e** GCD curves of the ASC at different current densities; **f** EIS curve of the ASC; **g** Ragone plot of the ASC and comparison with other materials; **h** cyclic stability test of the ASC for 5000 cycles at 20 mA cm^{-2}; **i** photographs of driven devices of one motor by the ASC in series

retain 64% of the original *Cs*, which shows its good rate performance.

To further evaluate the electrochemical performance of flexible ASCs, an EIS test was performed. Figure 5f, according to the fitting analysis, reveals that the device exhibits the low Rs of 1.94 Ω and the Rct of 2.91 Ω, indicating its good electrical conductivity. Meanwhile, the Ragone diagram presented in Fig. 5g depicts that the ASC demonstrates an energy density of 66.79 μWh cm^{-2} at a power density of 0.699 mW cm^{-2} and maintains 42.78 μWh cm^{-2} at 7 mW cm^{-2}. The performance of the ASC is compared with other devices in Table S2. It can be noticed that the ASC has a high energy density. The cycling stability was investigated through repeated GCD tests as shown in Fig. 5h, whereby the ASCs retained the 85.2% cycle stability at 20 mA cm^{-2} after 5000 cycles, indicating excellent cycling performance. In addition, as shown in Fig. 5i, three ASCs were connected in series to achieve a 4.2 V voltage range, successfully driving a motor. This demonstrates the practical application value of this ASC. The aforesaid results indicate that the Ni–Co LDH@CMS composites have great application potential in flexible energy storage devices.

In addition, we have applied flexible Ni–Co LDH@CMS composites to pressure sensors. When subjected to external pressure, the three-dimensional skeleton of Ni–Co LDH@CMS will deform, causing a change in the resistance value inside the material and resulting in an electrical output. The sensitivity of the Ni–Co LDH@CMS pressure sensor can be represented by the slope of its curve in Fig. 6a. It exhibits a sensitivity of 0.95 kPa^{-1} in the low-pressure region (0–20 kPa) and 6.49 kPa^{-1} in the high-pressure region (20–33 kPa). Moreover, as illustrated in Fig. 6b, the Ni–Co LDH@CMS pressure sensor has a very short response time and recovery time (both around 20 ms), indicating an extremely fast response speed. To verify the stability of the sensor, we have conducted 5000 cycle tests. Figure 6c shows that

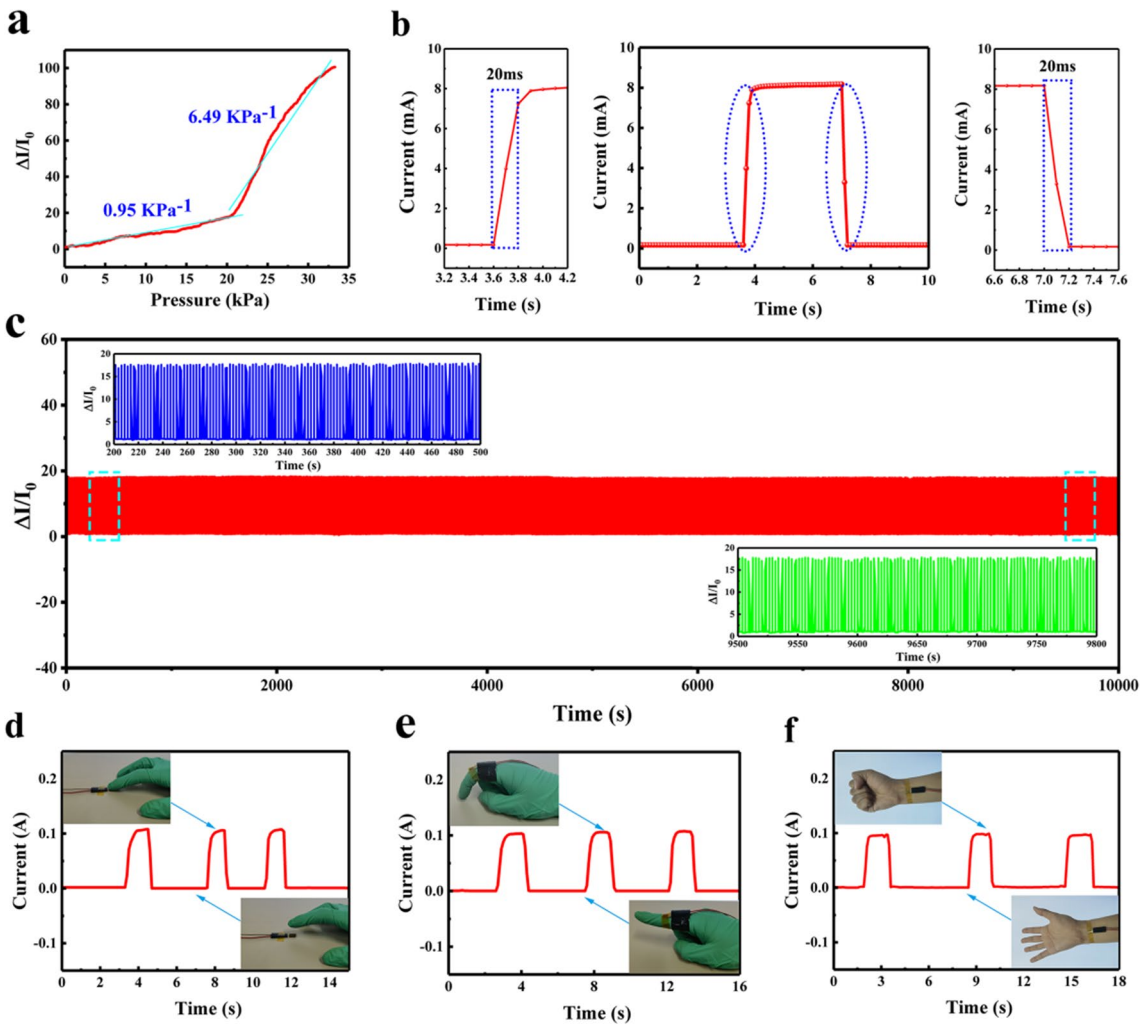

Fig. 6 **a** Current response of Ni–Co LDH@CMS sensor under different pressures (1–33 kPa); **b** response time and recovery time of the sensor; **c** cycling stability test of the sensor under 20 kPa for 5000 cycles; the i–t curves of Ni–Co LDH@CMS sensor originate from **d** finger press, **e** finger curvature, and **f** palmar extension

no significant current attenuation occurs, indicating its good stability. Notably, the Ni–Co LDH@CMS pressure sensor can detect human body movements and has a wide range of applications. As displayed in Fig. 6d, when gently pressed with a finger, the intensity and duration of the pressure can be clearly observed from its current curve. Figure 6e, f demonstrates that it can monitor human joint movements, such as finger curvature and palmar extension. Consequently, Ni–Co LDH@CMS composites hold great potential in the field of pressure sensors.

Conclusions

In summary, melamine sponge was carbonized, and a dense Ni–Co LDH nanoflake structure was grown on its surface by hydrothermal reaction. Based on the synergistic effect between Ni–Co LDH and CMS, synthesized Ni–Co LDH@CMS composite not only has high *Cs*, but also retains the original flexibility of melamine sponge. At the same time, the Ni–Co LDH nanoflakes are closely arranged, which not only increases a large number of chemical reaction active sites, but also shortens the transmission distance of ions in the electrolyte, making the faradaic redox reaction on the electrode material surface more sufficient. Ni–Co LDH@CMS composite exhibits a high *Cs* of 2039.8 mF cm^{-2} at 1 mA cm^{-2}. Furthermore, an all-solid-state flexible ASC is assembled by Ni–Co LDH@CMS cathode material. The device exhibits 66.79 μWh cm^{-2} energy density at 0.699 mW cm^{-2} power density. After 5000 cycles, the capacity retention rate of the ASC is 85.2%. Similarly, the Ni–Co LDH@CMS composite material is applied to the pressure sensor, which also showed excellent stability and application prospects.

Supplementary Information The online version contains supplementary material available at https://doi.org/10.1007/s11581-023-05133-5.

Author contribution Hexiang Hu: writing (original draft preparation), investigation, and data curation; Jialun Li, Yi Jiang: data curation and investigation; Liying Wang and Xuesong Li: writing (reviewing and editing), project administration, and funding acquisition; Xijia Yang and Wei Lü: validation, supervision, project administration, resources, and funding acquisition.

Funding This work was financially supported by the National Natural Science Foundation of China (No. 62004014 and 62004015) and the Department of Science and Technology of Jilin Province (20210101077JC and 20230101330JC).

Data availability The data generated and/or analyzed during the current study are not publicly available for legal/ethical reasons but are available from the corresponding author on reasonable request.

Declarations

Competing interests The authors declare no competing interests.

References

1. Hou X, Zhang Q, Wang L, Gao G, Lu W (2021) Low-temperature-resistant flexible solid supercapacitors based on organohydrogel electrolytes and microvoid-incorporated reduced graphene oxide electrodes. ACS Appl Mater Interfaces 13(10):12432–12441
2. Isaac JA, Devaux D, Bouchet R (2022) Dense inorganic electrolyte particles as a lever to promote composite electrolyte conductivity. Nat Mater 21(12):1412–1418
3. Kumar R, Pérez del Pino A, Sahoo S, Singh RK, Tan WK, Kar KK, Matsuda A, Joanni E (2022) Laser processing of graphene and related materials for energy storage: state of the art and future prospects. Prog Energy Combust Sci 91:100981
4. Han C, Ding X, Zhu J (2023) Construction of $CoNi_2S_4$/nitrogen-doped lignite-based porous carbon composites and their application in supercapacitors. Ionics 29(3):1199–1207
5. Shang Y, Ma S, Wei Y, Yang H, Xu Z (2020) Flower-like ternary metal of Ni-Co-Mn hydroxide combined with carbon nanotube for supercapacitor. Ionics 26(7):3609–3619
6. Duan L, Zhao L, Cong H, Zhang X, Lu W, Xue C (2019) Plasma treatment for nitrogen-doped 3D graphene framework by a conductive matrix with sulfur for high-performance Li-S batteries. Small 15(7):1804347–1804355
7. Shi L-A, Ge J, Hu B-C, Ma T, Zhao H, Song Y-H, Li C, Yu S-H (2021) Joule-heated carbonized melamine sponge for high-speed absorption of viscous oil spills. Nano Res 14(8):2697–2702
8. Zhang XY, Sun SH, Sun XJ, Zhao YR, Chen L, Yang Y, Lu W, Li DB (2016) Plasma-induced, nitrogen-doped graphene-based aerogels for high-performance supercapacitors. Light Sci Appl 5(10):16130–16137
9. Zhang T, Sun Y, Wang X, Xiao L (2023) Design and fabrication of cactus-like $ZnCo_2O_4$@$Ni(OH)_2$ core/shell nanosheet arrays electrode for asymmetric supercapacitors. Ionics 29(5):2065–2073
10. Zhao C, Tian S, Nie P, Deng T, Ren F, Chang L (2019) Electrodeposited binder-free CoMn LDH/CFP electrode with high electrochemical performance for asymmetric supercapacitor. Ionics 26(3):1389–1396
11. Daneshvar S, Arvand M (2020) In-situ growth of hierarchical Ni–Co LDH/$CoMoO_4$ nanosheets arrays on Ni foam for pseudocapacitors with robust cycle stability. J Alloys Compd 815:152421
12. Wani TA, Suresh G (2021) A comprehensive review of $LiMnPO_4$ based cathode materials for lithium-ion batteries: current strategies to improve its performance. J Energy Storage 44:103307
13. Li X, Li X, Ting L, Lu Y, Shang C, Ding X, Zhang J, Feng Y, Xu FJ (2021) Wearable, washable, and highly sensitive piezoresistive pressure sensor based on a 3D sponge network for real-time monitoring human body activities. ACS Appl Mater Interfaces 13(39):46848–46857
14. Bai T, Wang W, Xue G, Li S, Guo W, Ye M, Wu C (2021) Free-standing, flexible Carbon@MXene films with cross-linked mesoporous structures toward supercapacitors and pressure sensors. ACS Appl Mater Interfaces 13(48):57576–57587
15. Peng Z, Yu C, Zhong W (2022) Facile preparation of a 3D porous aligned graphene-based wall network architecture by confined self-assembly with shape memory for artificial muscle, pressure sensor, and flexible supercapacitor. ACS Appl Mater Interfaces 14(15):17739–17753
16. Acharya J, Park M, Ko TH, Kim B-S (2021) Leaf-like integrated hierarchical $NiCo_2O_4$ nanorods@Ni-Co-LDH nanosheets electrodes for high-rate asymmetric supercapacitors. J Alloys Compd 884:161165
17. Han E, Han Y, Zhu L, Yang P, Du X (2017) Polyvinyl pyrrolidone-assisted synthesis of flower-like nickel-cobalt layered double hydroxide on Ni foam for high-performance hybrid supercapacitor. Ionics 24(9):2705–2715
18. Li J, Feng Y, Cao M, Yang L, Yao J (2021) Direct coating pen ink carbon on a carbonized melamine sponge as a flexible free-standing electrode. Ind Eng Chem Res 60(9):3597–3604
19. Liu T, Qu Y, Liu J, Zhang L, Cheng B, Yu J (2021) Core-shell structured C@SiO_2 hollow spheres decorated with nickel nanoparticles as anode materials for lithium-ion batteries. Small 17(49):2103673
20. Selvaraj AR, Raja IS, Chinnadurai D, Rajendiran R, Cho I, Han DW, Prabakar K (2022) Electrospun one dimensional (1D) pseudocapacitive nanorods embedded carbon nanofiber as positrode and graphene wrapped carbon nanofiber as negatrode for enhanced electrochemical energy storage. J Energy Storage 46:103731
21. Zhang Y, Xue S-c, Yan X-h, Gao H-l, Jing X, Gao K-z, Cao Y, Luo H-w, Yan J (2022) Synthesis of CoAl-LDH@$Ni(OH)_2$ high-performance supercapacitor electrode composites by hydrothermal-assisted electrodeposition. Ionics 28(11):5211–5222
22. Li H, Lin S, Li H, Wu Z, Chen Q, Zhu L, Li C, Zhu X, Sun Y (2022) Magneto-electrodeposition of 3D cross-linked NiCo-LDH for flexible high-performance supercapacitors. Small Methods 6(3):2101320
23. Liang H, Lin J, Jia H, Chen S, Qi J, Cao J, Lin T, Fei W, Feng J (2018) Hierarchical NiCo-LDH@NiOOH core-shell heterostructure on carbon fiber cloth as battery-like electrode for supercapacitor. J Power Sources 378:248–254
24. Ramandi S, Entezari MH (2022) Self-supporting electrode for flexible supercapacitors: NiCo-layered double hydroxide derived from metal organic frameworks wrapped on graphene/polyaniline nanotubes@cotton cloth. J Energy Storage 56:106106
25. Zhang C, Zhang L, Liu Q, Ding Y, Cheng L, Wu M, Li Z (2022) Enhanced interfacial electron transfer by constructing NiCo-LDH hollow nanocages decorated N-doped graphene quantum dots heterojunction for high-performance supercapacitors. Appl Surf Sci 602:154352
26. Zhao T, Liu C, Meng T, Deng W, Zheng L, Yi F, Gao A, Shu D (2022) Graphene quantum dots pinned on nanosheets-assembled NiCo-LDH hollow micro-tunnels: toward high-performance pouch-type supercapacitor via the regulated electron localization. Small 18(20):2201286
27. Feng Y, Cao M, Yang L, Zhang X-F, Wang Y, Yu D, Gu X, Yao J (2018) Bilayer N-doped carbon derived from furfuryl alcohol-wrapped melamine sponge as high-performance supercapacitor. J Electroanal Chem 823:633–637

28. Luo L, Zhou Y, Yan W, Luo L, Deng J, Du G, Fan M, Zhao W (2021) Design and construction of hierarchical sea urchin-like NiCo-LDH@ACF composites for high-performance supercapacitors. Ind Crop Prod 171:113900
29. Wang X, Li X, Huang C, Hao C, Ge C, Guo Y (2020) Fabrication of NiCoAl-layered double hydroxide/N-GO for high energy all-solid-state asymmetric supercapacitors. Appl Surf Sci 527:146891
30. Xu M, Ma Y, Liu R, Liu Y, Bai Y, Wang X, Huang Y, Yuan G (2020) Melamine sponge modified by graphene/polypyrrole as highly compressible supercapacitor electrodes. Synth Met 267:116461
31. Zhang L, Cai P, Wei Z, Liu T, Yu J, Al-Ghamdi AA, Wageh S (2021) Synthesis of reduced graphene oxide supported nickel-cobalt-layered double hydroxide nanosheets for supercapacitors. J Colloid Interface Sci 588:637–645
32. Zou J, Xie D, Xu J, Song X, Zeng X, Wang H, Zhao F (2022) Rational design of honeycomb Ni-Co LDH/graphene composite for remarkable supercapacitor via ultrafast microwave synthesis. Appl Surf Sci 571:151322
33. Sun B, Fan X, Hou R, Zhao G, Liu Q, Zhou H, Liang P (2023) Electrode made of NiCo double hydroxide on oxidized activated carbon for asymmetric supercapacitors. Chem Eng J 454:140280
34. Shan Q, Huo W, Shen M, Jing C, Peng Y, Pu H, Zhang Y (2020) Melamine sponge derived porous carbon monoliths with NiMn oxides for high performance supercapacitor. Chin Chem Lett 31(9):2245–2248
35. Cao C-F, Liu W-J, Xu H, Yu K-X, Gong L-X, Guo B-F, Li Y-T, Feng X-L, Lv L-Y, Pan H-T, Zhao L, Li J-Y, Gao J-F, Zhang G-D, Tang L-C (2021) Temperature-induced resistance transition behaviors of melamine sponge composites wrapped with different graphene oxide derivatives. J Mater Sci Technol 85:194–204
36. Stejskal J, Sapurina I, Vilčáková J, Humpolíček P, Truong TH, Shishov MA, Trchová M, Kopecký D, Kolská Z, Prokeš J, Křivka I (2021) Conducting polypyrrole-coated macroporous melamine sponges: a simple toy or an advanced material? Chem Pap 75(10):5035–5055
37. Wang Z, Yu H, Xiao Y, Guo L, Zhang L, Dong X (2021) Polydopamine mediated modification of manganese oxide on melamine sponge for photothermocatalysis of gaseous formaldehyde. J Hazard Mater 407:124795
38. Xue J, Zhu L, Zhu X, Li H, Ma C, Yu S, Sun D, Xia F, Xue Q (2021) Tetradecylamine-MXene functionalized melamine sponge for effective oil/water separation and selective oil adsorption. Sep Purif Technol 259:118106
39. Yuan W, Liu H, Wang X, Huang L, Yin F, Yuan Y (2021) Conductive MXene/melamine sponge combined with 3D printing resin base prepared as an electromagnetic interferences shielding switch. Compos A: Appl Sci Manuf 143:106238
40. Jia H, Zhu J, Zhang M, Sang S, Hu F, Zhang F (2021) Fluorine and nitrogen co-doped mesoporous carbon derived from polytetrafluoroethylene@melamine sponge for supercapacitor application. J Energy Storage 38:102631
41. Jing X, Wang L, Qu K, Li R, Kang W, Li H, Xiong S (2021) KOH chemical-activated porous carbon sponges for monolithic supercapacitor electrodes. ACS Appl Energy Mater 4(7):6768–6776
42. Li S, Chang Y, Han G, Song H, Chang Y, Xiao Y (2019) Asymmetric supercapacitor based on reduced graphene oxide/MnO_2 and polypyrrole deposited on carbon foam derived from melamine sponge. J Phys Chem Solids 130:100–110
43. Shi Y, Liu G, Jin R, Xu H, Wang Q, Gao S (2019) Carbon materials from melamine sponges for supercapacitors and lithium battery electrode materials: a review. Carbon Energy 1(2):253–275
44. Zhang J, Chen G, Zhang Q, Kang F, You B (2015) Self-assembly synthesis of N-doped carbon aerogels for supercapacitor and electrocatalytic oxygen reduction. ACS Appl Mater Interfaces 7(23):12760–12766
45. Huang S, Zhang X, Yang X, Wang L, Li X, Lü W (2021) Preparation of carbonized sponge/MnO_2 composite for energy storage application. Ionics 27(5):2089–2095
46. Du H, Ding F, Zhao J, Zhang X, Li Y, Zhang Y, Li J, Yang X, Li K, Yang Y (2020) Core-shell structured Ni_3S_2@VO_2 nanorods grown on nickel foam as battery-type materials for supercapacitors. Appl Surf Sci 508:144876
47. Li S, Luo Y, Wang C, Wu M, Xue Y, Yang J, Li L (2022) A novel hierarchical core-shell structure of $NiCo_2O_4$@NiCo-LDH nanoarrays for higher-performance flexible all-solid-state supercapacitor electrode materials. J Alloys Compd 920:165986
48. Liu Y, Wang Y, Shi C, Chen Y, Li D, He Z, Wang C, Guo L, Ma J (2020) Co-ZIF derived porous NiCo-LDH nanosheets/N doped carbon foam for high-performance supercapacitor. Carbon 165:129–138
49. Zhu F, Liu W, Liu Y, Shi W (2020) Construction of porous interface on CNTs@NiCo-LDH core-shell nanotube arrays for supercapacitor applications. Chem Eng J 383:123150